ACS OMEGA

http://pubs.acs.org/journal/acsodf

Article

Synthesis of FAU-Zeolite Membrane by a Secondary Growth Method: Influence of Seeding on Membrane Growth and Its Performance in the Dehydration of Isopropyl Alcohol−Water Mixture

Masahiko Matsukata,* Yasushi Sekine, Eiichi Kikuchi, Motomu Sakai, Bharathi Subramanian, Makoto Toyoda, and Taisuke Furuhata

Cite This: *ACS Omega* 2021, 6, 9834−9842

Read Online

ACCESS | Metrics & More | Article Recommendations | Supporting Information

ABSTRACT: Y-type zeolite membranes were prepared on a porous tubular α-alumina support by a secondary growth process. Various experimental conditions such as seed size, pH of seed solution, and degassing of support were examined for understanding their influence on the membrane deposition process. The experimental results showed that the potential of alumina support surface and the USY seed slurry plays a significant role in controlling the electrostatic interaction between seed particles and support surface and also the aggregation of USY seed particles in the slurry. In addition, we also noted the significance of the capillary forces working at the three-phase interface on the support surface and is a key factor that governs the seeding behavior onto the tubular support surface. Optimization of these parameters resulted in crack-free compact membranes that were able to effectively separate a mixture of isopropyl alcohol and water in a vapor-phase separation process.

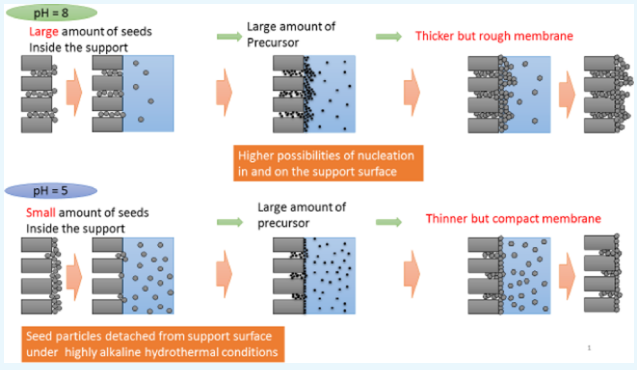

INTRODUCTION

Zeolite membrane-based separation is gaining momentum in chemical and pharmaceutical industries owing to its ability to reduce the energy cost significantly by increasing the efficiency and selectivity of separation and purification process.[1] Availability of various kinds of zeolites with wide ranges of micropore size and shape, adsorption, and ion exchange capacity makes zeolite an attractive membrane material for separation of gas mixtures and liquids with close boiling points.[2−4] Zeolite-based membranes have been used for the separation of gas mixtures such as CO_2/N_2, CO/H_2, and liquids like alcohol−water mixture[5−15] and aromatic solvents[16,17]

Dehydration of isopropyl alcohol (IPA) is one of the industrially relevant processes, in which zeolite membrane-based process offers significant energy saving. IPA is an important solvent, cleaning agent, and chemical intermediate and is extensively used in semiconductor, chemical, and pharmaceutical industries. Industrial requirement for water content in IPA is less than 0.05% (by wt). However, the current production process produces an azeotropic mixture of IPA and water, as the water content is always higher than 10%. Separation of this azeotropic mixture consumes significant energy and accounts for the nearly 35% of the total energy cost of the IPA production process. Hence, introducing a zeolite membrane separator can result in enormous reduction in the energy consumption/cost. Commercially available LTA membrane is not suitable for the dehydration of IPA in the presence of a large water content in the mixture,[17] as LTA membrane deteriorates in the presence of large water content in the mixture. Thus, we were motivated to find an alternative zeolite membrane that can withstand a large water vapor concentration, unlike an LTA-type zeolite membrane, for a distillation−membrane hybrid system to separate water and IPA.

Membrane for this system requires a high flux of water, high permselectivity to water, and resistant to water. Faujasite type (FAU), zeolite Y, has all of these characteristics because of its Si/Al ratio in the range of 1.5−3 and a large pore made of 12-membered rings. There are studies involving Y-type zeolite membrane for the dehydration of organic substance and

Received: January 28, 2021
Accepted: March 22, 2021
Published: March 31, 2021

https://doi.org/10.1021/acsomega.1c00513
ACS Omega 2021, 6, 9834−9842

separation of binary gases or organic substances.[18−21] Kita et al.[22] and Kumakiri et al.[23] have reported that zeolite Y membrane was highly selective to water in water/ethanol mixtures.

FAU-zeolite membranes have been synthesized by a secondary growth method on a porous ceramic support seeded with zeolite crystals. Further, most of FAU membranes used in separation studies, so far, involved only mild solvents with a low water content (less than 10%). Verweij et al. have studied the electrostatic interaction between the alumina support and slurry by measuring the ζ potential of seed slurry and showed the role played by the surface charges on the adhesion of seed to support.[24] However, a systematic study relating to the seeding conditions with membrane performance is still lacking. Another major concern with zeolite membrane, in general, is the reproducibility of the membrane formation process. Extremely divergent results have been obtained for the same mixture and membrane system.[25−27] For example, Chen et al.[25] reported a mordenite membrane for water/IPA system under pervaporation conditions. Their membrane showed a high separation factor of around 10 000 when the water content in the mixture was around 10%. This unfortunate diversity of experimental results can be attributed to the lack of knowledge about the membrane formation process. We have to take into account various parameters such as the nature of support, the porosity of support, and seeding conditions like seed size and the pH of seed solution. Understanding the interplay between these parameters is vital to control the microstructures of zeolite membrane and to synthesize membranes with improved and reproducible separation performance.

In this work, we have examined how the seeding process influences the subsequent membrane growth, which in turn influenced the separation efficiency. We synthesized the FAU membrane on porous α-alumina supports seeded using the seed solutions prepared at different values of pH and concentrations. Further, the performance of the membrane prepared under different conditions was evaluated by comparing with the performance of separating the IPA−water mixture.

RESULTS AND DISCUSSION

ζ-Potential and Mean Particle Size Measurement of Zeolite Seed Slurry. Figure 1 shows the ζ-potentials of USY seed slurry and α-alumina support as a function of pH. The ζ-potential of the α-alumina support became negative with increasing value of pH. Alumina support showed positive ζ potentials between pH = 3 and 10 and negative ζ potentials between pH = 10 and 12. The isoelectric point (IEP) of support lies between pH = 9 and 10. Figure 1 also gives the ζ-potentials of USY seed slurry at different concentrations and pH values. It can be seen from the figure that the ζ potential of slurry is negative at all of the pH values studied. This observation is similar to that reported by Verweij et al.[24] who have reported negative ζ potentials for commercially available USY zeolites (Si/Al ratio of 2.5) between pH = 1 and 11.5. The USY slurry in our studies showed negative ζ potential values in the whole pH range between 2 and 12. However, the extent of surface charges as seen from the absolute values of the ζ potential changed sharply between pH = 6 and 7. The USY zeolite seed slurry showed a negative ζ potential (−5 to −10 mV), indicating a weak surface charge density, at low pH values (2−6). A large shift to the ζ-potential (−50 mV) of

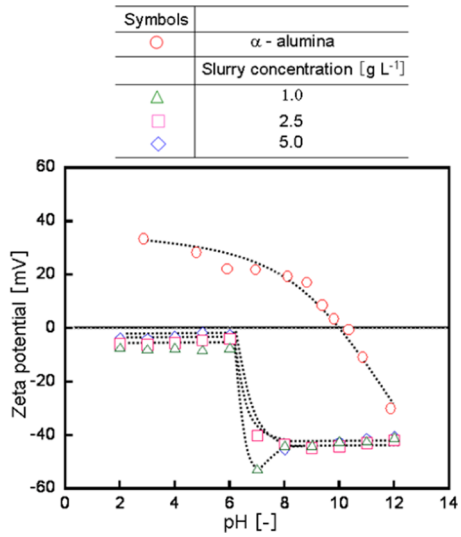

Figure 1. ζ Potentials of USY slurries and α-alumina support as a function of pH. The slurry concentrations were 1.0, 2.5, and 5.0 g L^{-1}.

slurry was observed at higher pH values (7−12) (Figure 1), indicating a high surface change density. This sharp change in the absolute value of ζ potential indicates that the surface charge density increased drastically between pH = 6 and 7. Judging from the ζ potentials of slurry and support at different pH values, we can expect the following phenomena.

1. Between pH = 2 and 6, the electrostatic force working between particles and support would be weak due to the fact that the ζ-potential of the slurry was weakly negative (close to zero surface charge) and the support surface was positively charged.
2. Between pH = 7 and 10, we can expect a strong electrostatic attraction between seed particles and support surface as evidenced from the positive and negative ζ potentials of support and seed, respectively.

Figure 2 gives the mean particle size of USY seed at different seed concentrations as a function of pH. Generally, when the absolute value of ζ-potential is small, the surface change density is very weak and may not be sufficient to keep particles separate. Hence, the seed particles aggregate by the action of

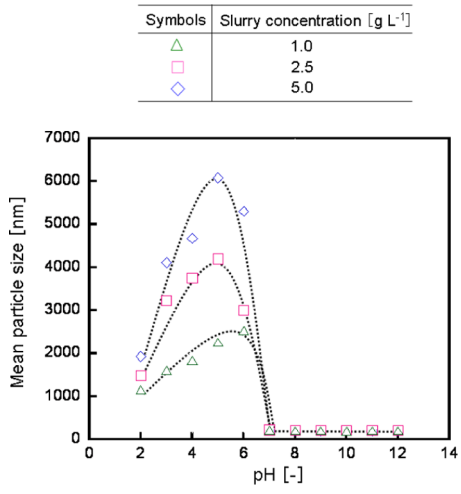

Figure 2. Mean particle sizes of USY slurries, at different concentrations, as a function of pH.

https://doi.org/10.1021/acsomega.1c00513
ACS Omega 2021, 6, 9834−9842

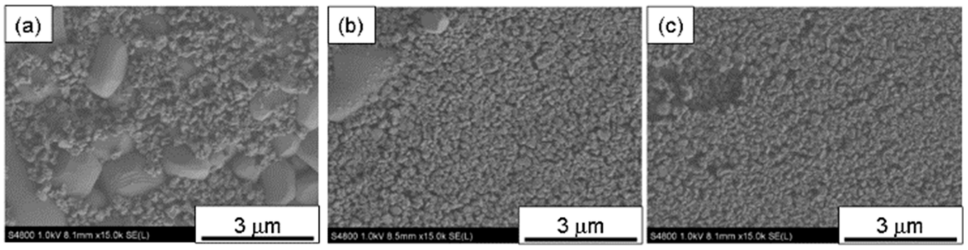

Figure 3. Typical FE-SEM images for the surface of seeded nonporous α-alumina plate at pH (a) 5, (b) 7, and (c) 8. Seed slurry concentration = 5.0 g L^{-1}.

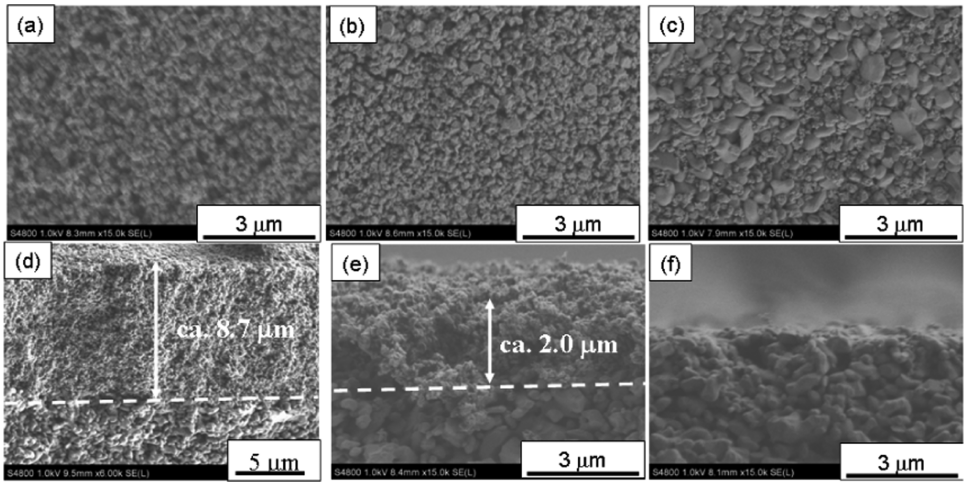

Figure 4. Typical FE-SEM images of seeded α-alumina supports at different pH values. Slurry concentration = 5.0 g L^{-1}; (a–c) surface images; (d–f) cross-sectional images; pH of USY seed slurry: (a, d) 5, (b, e) 7, and (c, f) 8.

van der Waals force and the extent of aggregation increased with increasing concentration.

This trend is observed in all three seed concentrations as seen by the increase in the average particle size of slurry from about 1–2 to 2–6 μm when the seed concentration was increased from 1 to 5 g L^{-1} (between pH 2 and 6). Between pH 7 and 12, the average particle size of seeds remained constant (at 0.15 μm) irrespective of the seed concentration. This monodispersion at high pH was attributed to a large repulsive force between particles as evidenced by the higher value of absolute ζ potential. Thus, these results indicated that between pH 2 and 6, the seed slurry contained aggregated particles ranging from 1 to 6 μm depending on the seed concentration and the pH of slurry. However, between pH 7 and 12, no aggregation was observed and the apparent seed size remained the same at about 0.15 μm irrespective of its concentration.

Dip Coating of Seeds. *Dip Coating on Nonporous α-Alumina Plate.* To understand the seeding behavior, we need to understand the interaction between seed particle and porous alumina support. Surface charge and porosity of the alumina support are two main factors determining the extent of the seed adsorption onto the support. Further, to explain the influence of porosity and surface charge, we compared the seeding behavior on nonporous and porous alumina support. The nonporous α-alumina plate (supplied by NORITAKE Ltd.) was used for seeding under identical conditions as those used to prepare the porous support.

The amount of seed on the α-alumina plate was followed by measuring the weight of plate before and after the seeding. The weight gain of α-alumina plate after the seeding from the slurry containing 1–5 g L^{-1} of seeds at pH = 5, 7, and 8 has revealed the following. Generally, the seed adsorption on the α-alumina plate increased with increasing pH. However, at pH = 5, the amount of seed on the plate (as revealed by weight gain) was independent of the amount of seed concentration (1–5 g L^{-1}), while at pH = 7 and 8, the amount of seed on the plate increased with increasing seed concentration. Figure 3 depicts typical field emission scanning electron microscope (FE-SEM) images of the α-alumina nonporous plate surface seeded at three different pH values, viz., 5, 7, and 8, from a slurry containing 5 g L^{-1} of zeolite. As seen from these FE-SEM images, at pH = 8, the USY seeds fully covered the plate surface. However, at pH = 5 and 7, the coverage of plate surface with the USY seed particles was incomplete. Bare support surface is still observed after the seeding. These observations of partial coverage at pH = 5 and 7 and complete coverage at pH = 8 indicate the contribution of electrostatic interaction between α-alumina surface and USY seed particles to the seeding behavior. Since at pH = 5 the ζ-potential of α-alumina surface was positive and that of USY particles was weakly negative (close to zero surface charge (Figure 1, ζ potential data)), there is weak electrostatic interaction between the α-alumina surface and slurry particles, leading to the formation of partially covered support. However, at higher pH = 8, the ζ-potential of α-alumina surface was positive and that of USY seed particles was negative. Under such conditions, a strong electrostatic attraction acted between the α-alumina surface and monodispersed USY seed particles, leading to the full coverage of alumina surface with seed particles.

Dip Coating on Porous α-Alumina Support. Figure 4 shows typical FE-SEM images of the surface and cross section

https://doi.org/10.1021/acsomega.1c00513
ACS Omega 2021, 6, 9834–9842

of α-alumina porous supports seeded with a slurry containing 5.0 g L^{-1}. Interestingly, as seen in Figure 4, markedly different seeding behavior was observed with porous α-alumina support. Unlike the seeding behavior on the nonporous α-alumina plate, FE-SEM images of the surface of porous support show that USY seeds fully covered the surface at pH = 5 and very little coverage at pH = 8. The cross-sectional views of support clearly show the formation of thick seed layers of about 9 and 2 μm at pH = 5 and 7, respectively. At pH = 8, no particles can be seen on the surface. However, the seed particles could be seen embedded inside the voids of alumina support. Figure 5

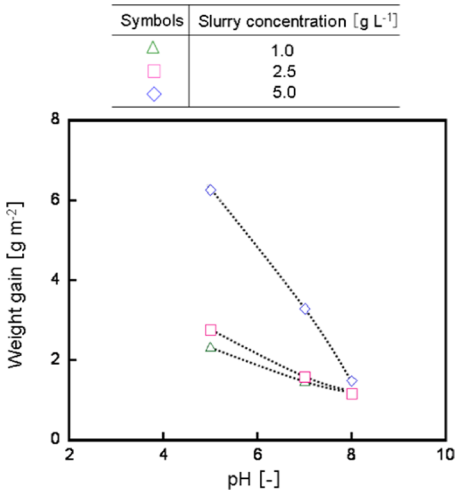

Figure 5. Weight gain of the α-alumina support after seeding as a function of pH at different seed concentrations.

illustrates the weight gain of α-alumina support after seeding with the solutions containing 1−5 g L^{-1} at three different pH values, viz., 5, 7, and 8. It can be seen from the figure that the weight gain obtained at different concentrations of the USY slurry follows a general trend. The values of weight gain are summarized in Table 1 in the Supporting Information. The weight gain of support at a given pH increased with increasing slurry concentration. On the other hand, for a given slurry concentration, weight gain decreased with increasing pH.

One can observe from the figure that at pH = 8, the weight gain was minimal and remained practically the same when the seed concentration increased from 1 to 5 g L^{-1}. However, at pH = 5, the weight gain with seed adsorption increased with increasing seed concentration as evidenced from increasing weight observed with increasing seed concentration. Such an observation along with FE-SEM suggested that all of the seeding took place on the top of surface support at pH = 5, while at pH = 8, all seeds were embedded inside the support, and the behavior at pH = 7 was intermediate since the seeds were located partly inside and outside the support.

This seeding behavior observed with porous α-alumina support was markedly different from that on the nonporous α-alumina plates and cannot be explained by the electrostatic interaction between α-alumina surface and USY seed particles. On the porous support, the pores of support possibly played a significant role in the adhesion behavior of seed particles onto the surface of porous support.

Dip-Coating Behavior on Degassed Support. We suppose that the different seeding behaviors on the nonporous and porous α-alumina supports might be due to the forces acting at the three-phase interface at the pores involving air inside the pores of support, the USY slurry solution, and the solid surface of α-alumina support.

To eliminate the influence of air inside the pores of support, we degassed (degassing procedure is given in the Supporting Information) the support prior to carrying out the dip coating on the tubular support. Figure 6 illustrates typical FE-SEM images of the surface of α-alumina support after the degassing and dip-coating at pH = 5 and 8. As can be seen from Figure 6, no seeding could be seen at pH = 5, while the complete coverage of support was observed at pH = 8. This trend was similar to that of seeding behavior on the nonporous alumina support and could be explained by the electrostatic interaction between the seed and support. Figure 7 compares the weight gain of different alumina support after seeding with seed solutions of 5 g L^{-1} at different pH values. The weight gain pattern of the degassed porous α-alumina support is very similar to that of the nonporous plate.

Based on these results, we propose a schematic representation of seeding as drawn in Figure 8. Seeding behavior on a porous support is governed by a combination of capillary and electrostatic forces. At low pH values between 2 and 7, the surface charge on the slurry particles is nearly zero or weekly negative. Hence, the seed particles tend to aggregate in solution and these aggregated particles were drawn onto porous support (without degassing) by capillary forces and fully covers the support. On the other hand, on the degassed support, at pH = 2 and 7, the electrostatic interaction between support and seed particles plays a predominant role.

In this pH range, the electrostatic attraction between particles and substrate is very weak; hence, seeding was difficult to occur on the degassed Al_2O_3 support. On the other hand, at pH = 8, the slurry particles remain dispersed without aggregation and, on a degassed support, are attracted toward

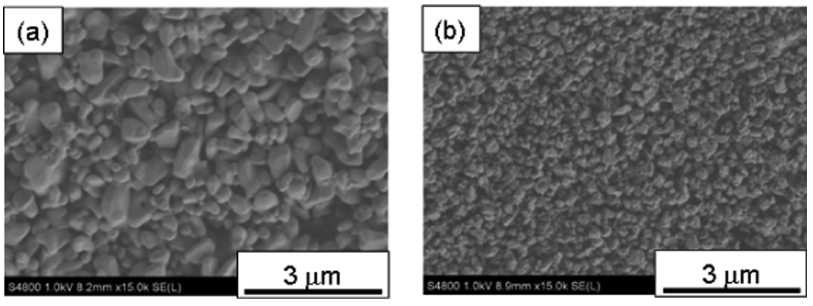

Figure 6. Typical FE-SEM images of the surface of degassed α-alumina support after seeding at (a) pH = 5 and (b) pH = 8. Slurry concentration = 5.0 g L^{-1}.

https://doi.org/10.1021/acsomega.1c00513
ACS Omega 2021, 6, 9834−9842

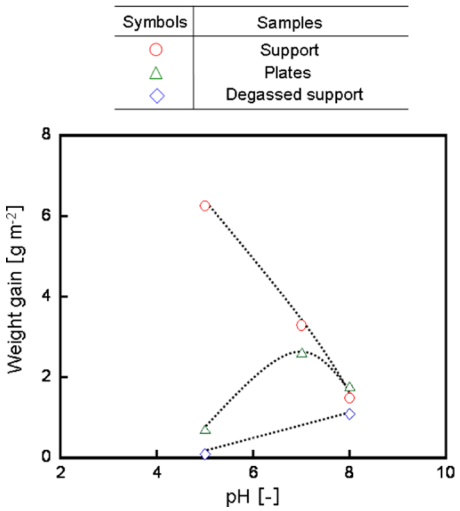

Figure 7. Comparison of weight gains of the degassed porous α-alumina support and the α-alumina plates after seeding as a function of pH. Slurry concentration = 5.0 g L^{-1}.

surface due to electrostatic forces and drawn inside the pores by the capillary forces (since the pore size of the support and particle size of the slurry are nearly the same, 0.15 μm), leading to the embedding of seeds inside pores of the support.

Membrane Formation Process. Figure 9 shows typical FE-SEM of surface and cross-sectional images of NaY membrane synthesized for 4 h on a tubular porous support (without degassing) seeded at pH = 5, 7, and 8, respectively. As seen from these images of membrane, thickness and roughness increased with increasing pH of the seed solution. It is interesting to note that the initial seed layer thickness follows an inverse trend, i.e., thickness of seed layer decreased as the seeding pH increased (Figure 4). It can be recalled that the total weight of seed on the support at a given seed concentration decreased with increasing pH (Figure 5).

However, the distribution of seeds on the support was significantly different. For instance, the weight gain at pH 8 was about 1.8−2.0 g m^{-2}, of geometric surface area, though, no seed particles were visible on the support surface (Figure 4c,f), suggesting that all of the seed particles were embedded inside the support pores. On the other hand, at pH = 5, a weight gain of 2.0−6.5 g m^{-2} was observed (Figure 5). The FE-SEM image of the support surface shows a large seed layer of a few microns on the support surface (Figure 4a,d), indicating that most of the seed particles were located on the support surface.

We examined the membrane growth process further, in detail, by observing the cross-sectional FE-SEM images of the support during different stages of membrane growth. Figures 10 and 11 show the membrane grown on a support seeded at pH = 5 and 8, respectively, at different deposition times ranging from 0 to 4 h. As can be seen from the FE-SEM images (Figure 9), the support seeded at pH = 5 started with a seed layer thickness of about 9 μm, while most of them disappeared during the first 30 min. A small amount of zeolite precursor appeared after 2 h of synthesis and a compact layer of membrane was formed after 4 h.

On the other hand, the support seeded at pH = 8 did not have any significant seeds on its surface. Despite this, a dense layer of zeolite precursor started growing within 1 h of membrane growth (Figure 10). Seemingly different growth patterns can be understood as follows. As explained earlier, when the seeding was carried out at pH = 5, most of the particles were in an aggregated form and bound loosely onto the support by the capillary forces, and these were easily detached from the support when immersed in the synthesis gel having a high pH > 14. At this pH, both particles and surface have a negative surface charge (vide infra ζ potential). Hence, the zeolite nucleation had to start from the synthesis gel in the absence of seeds on the support.

When the support was seeded at pH = 8, most of the seed particles were located inside the pores of support and acted as nucleation sites for the further zeolite growth as evidenced from the dense precursor observed within 2 h inside the membrane growth gel, resulting in the faster growth and a thicker film on the support. These results strongly suggested that the location of zeolite seed is important in determining the growth and compactness of subsequent membrane growth. A manuscript detailing this aspect is currently under preparation will be communicated shortly.

Vapor Permeation Measurements. To check the membrane quality, we evaluated their separation performance for IPA−water mixture. Figure 12 shows the permeances and separation factors of water and IPA through Y-type zeolite membranes as a function of membrane temperature. The water

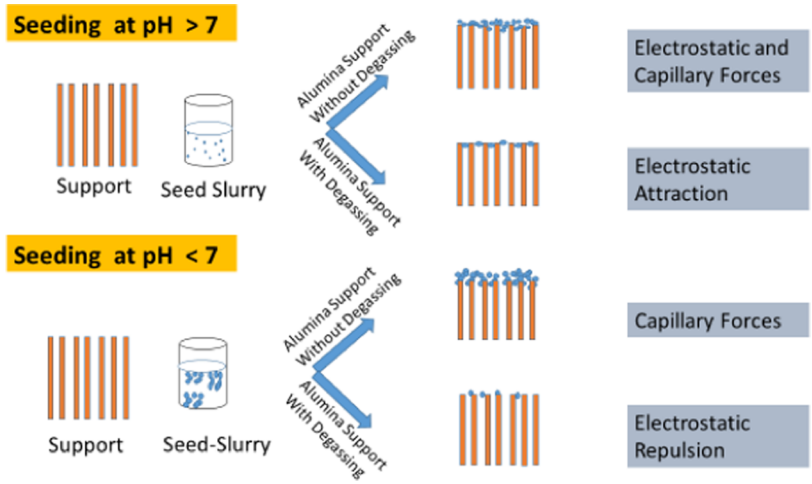

Figure 8. Model of seeding behavior on porous support.

https://doi.org/10.1021/acsomega.1c00513
ACS Omega 2021, 6, 9834−9842

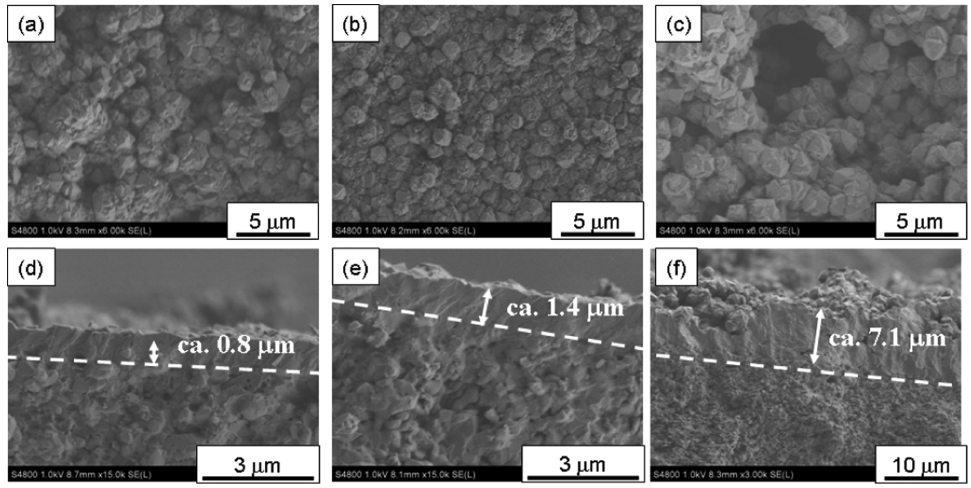

Figure 9. Typical FE-SEM images of NaY membranes: (a–c) surface images and (d–f) cross-sectional images. Slurry concentration = 5.0 g L^{-1}. Seeding by dip coating at (a, d) pH = 5, (b, e) pH = 7, and (c, f) pH = 8.

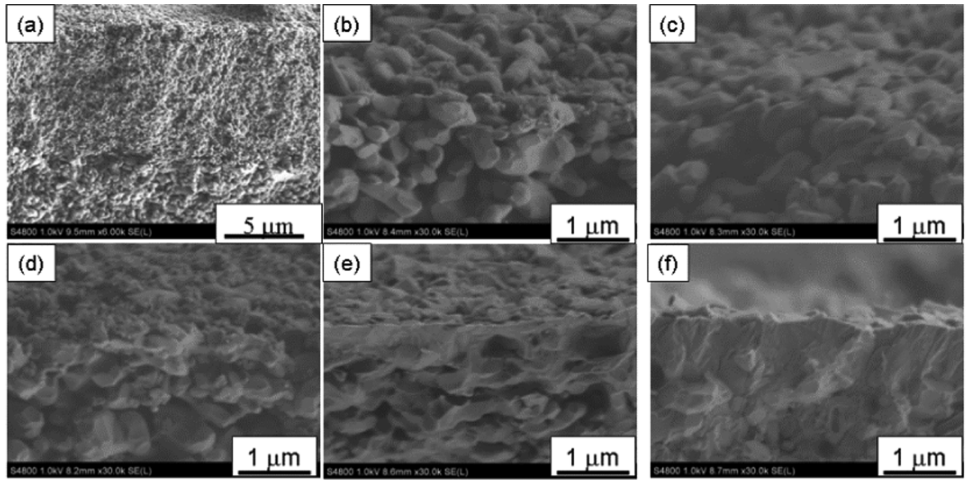

Figure 10. Typical cross-sectional FE-SEM images of NaY membranes. Dip coating was carried out at pH = 5. Slurry concentration = 5.0 g L^{-1}; crystallization period: (a) 0 h (after dip coating), (b) 30 min, (c) 1 h, (d) 2 h, (e) 3 h, and (f) 4 h.

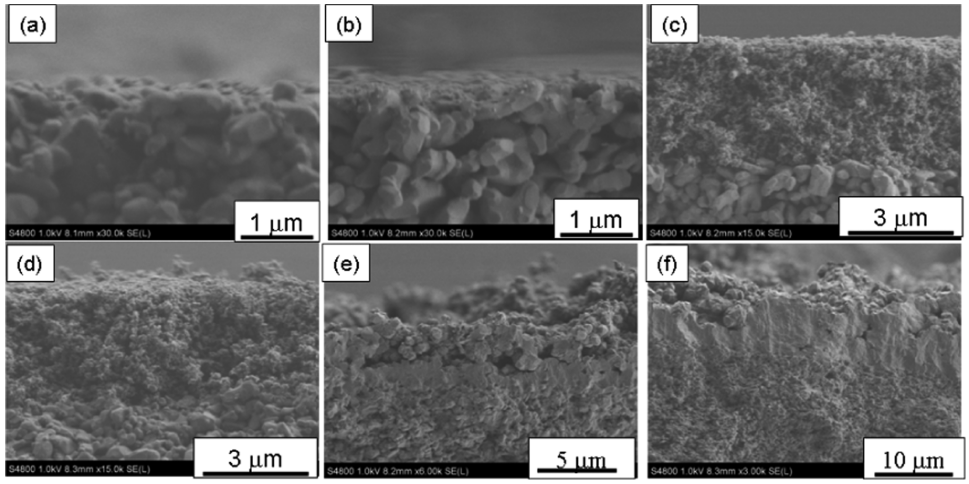

Figure 11. Typical cross-sectional FE-SEM images of NaY membranes. Dip coating was carried out at pH = 8. Slurry concentration = 5.0 g L^{-1}; crystallization period: (a) 0 h (after dip coating), (b) 30 min, (c) 1 h, (d) 2 h, (e) 3 h, and (f) 4 h.

permeances through different Y-type zeolite membranes tested in this study remained more or less constant at 7–8 × 10^{-7} mol m^{-2} s^{-1} Pa^{-1} and were independent of the temperature. This is obviously due to the hydrophilic nature of zeolite membrane, resulting in saturation of the Y-type zeolite membranes with water. However, the permeance of IPA

https://doi.org/10.1021/acsomega.1c00513
ACS Omega 2021, 6, 9834–9842

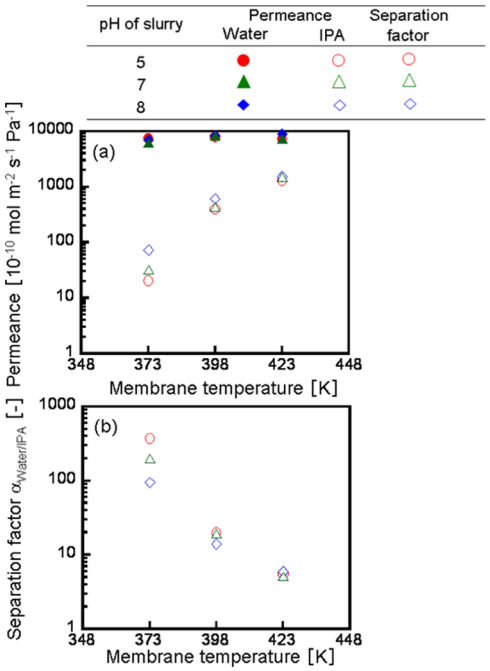

Figure 12. (a) Permeances of water and IPA and (b) separation factor through NaY membranes as a function of membrane temperature. Slurry concentration = 5.0 g L^{-1}.

increased with increasing temperature. The membrane grown on the support seeded at pH = 5 showed the lowest IPA permeance and hence the largest separation factor of 367 at 373 K. On the other hand, the membrane grown on the support seeded at pH = 8 showed a higher IPA permeance with a lower separation factor, α = 95, at 373 K. The membrane grown on the substrate seeded at pH = 8 was thicker than that of membrane grown on the substrate seeded at pH = 5, indicating that the former thicker membrane contained nonzeolitic pathways among zeolite crystals. In other words, synthesis conditions to grow a thicker zeolite layer are not always suitable to prepare a less defective and highly selective membrane. It should be more important to optimize the synthetic conditions to form a densely grown zeolite crystal layer on the basis of proper understanding of its formation pathways.

CONCLUSIONS

The seeding mechanism of USY seed particles on the tubular α-alumina porous support was investigated. We found, from the results of the ζ-potential measurements for an alumina support surface and USY seed slurry, that the electrostatic interaction between seed particles and support surface is important and governs both the adhesion of seed to support and the agglomeration USY seed particles in the slurry. In addition, we found that the capillary force working at the three-phase interface on the support surface, air in the pore of support, and the USY seed slurry is an overwhelming factor governing seeding behavior onto the tubular porous support surface. Our studies have shown that the compactness of membrane depends on the location of seeds on the support. When the seeds were predominantly located on the support surface, a thinner and compact membrane is produced. A thicker and less compact membrane was obtained when the seeds were located inside the pores of support.

EXPERIMENTAL SECTION

ζ-Potential and Mean Particle Size. We used ultrastable Y (USY, SiO_2/Al_2O_3 = 13.8, HSZ-360HUA, Tosoh Co.) zeolites as seeds. ζ-Potentials and mean particle sizes of the USY seed slurry and the porous α-alumina disk were measured using a ζ-potential and particle size analyzer (ELSZ-2 series, Otsuka Electronics Co.) at room temperature. ζ-Potential was determined by a laser Doppler method, and mean particle size was determined by a dynamic light scattering method. A disk-type porous α-alumina square support (10 mm × 10 mm) having an average pore diameter of 0.15 μm was obtained from NORITAKE Ltd. and used for the ζ-potential measurement of porous support surface. Similarly, a nonporous support also supplied by NORITAKE Ltd. was used for the ζ potential measurement of nonporous support.

USY seed slurry was prepared by grounding USY powder in a ball mill. The resultant particles were then dispersed in water. Small particles dispersed in water were recovered by centrifugal separation at 4000 rpm for 10 min. The small particles were redispersed in water again under ultrasonication. The concentrations of USY seed slurry were adjusted to 1.0, 2.5, and 5.0 g L^{-1}. The pH of the seed slurry was adjusted using hydrochloric acid (35.0%, Kanto Chemical Co.) and sodium hydroxide (97.0%, Kanto Chemical Co.).

Dip-Coating of Seed Particles. NaY membranes were prepared by a secondary growth method on the outer surface of porous α-alumina tubular support (inner diameter = 7 mm, outer diameter = 10 mm, length = 30 mm, and average pore size = 0.15 μm, supplied by NORITAKE Ltd.). The average pore diameter of tubular support was the same as the porous disk used for the ζ-potential measurement.

Seeding was carried out by a dip-coating method. The pH of USY seed slurry was adjusted to 5, 7, and 8, respectively. The seeding of α-alumina support was carried out as follows. Both ends of the tubular support were plugged with a Teflon rod to avoid penetration of slurry into the inner side of the tube. The support was vertically dipped in the USY slurry for 3 min, and the slurry was withdrawn vertically at 3 cm min^{-1}. Then, the dip-coated support was dried for 20 min at 293 K, subsequently for 2 h at 343 K. This procedure was repeated up to four times. The weights of samples before and after seeding and drying in an oven overnight were measured. The amount of seeds attached on the α-alumina support was evaluated as the amount of seeds attached per unit of the geometric surface area of alumina. In the case of tubular porous α-alumina support, the outer surface area of the tube was used in the calculation for normalization and the inner surface of support was not taken into account.

Membrane Synthesis. Seeded supports were immersed vertically in a polypropylene (PP) bottle filled with a synthesis gel. The synthesis gel was obtained using distilled water, sodium hydroxide (97.0 wt %, Kanto Chemical Co.), sodium silicate solution (SiO_2; 28−30 wt %, Na_2O; 9−10 wt % Kishida Chemical Co.), and sodium aluminate (Na_2O; 31−35 wt %, Al_2O_3; 34−39 wt % Kanto Chemical Co.), and its molar composition was $22Na_2O:Al_2O_3:25SiO_2:990H_2O$.[21] The synthesis gel was aged under stirring at room temperature for 4 h prior to use. The hydrothermal treatment was carried out under stirring at 373 K for 4 h. After crystallization, the membrane obtained was washed with distilled water and dried at 343 K overnight.

https://doi.org/10.1021/acsomega.1c00513
ACS Omega 2021, 6, 9834−9842

Characterization. The morphological features of the support and the zeolite seed layer were observed by a field emission scanning electron microscope (FE-SEM, Hitachi S4800) operated at 15 keV.

Vapor Permeation Measurements. Vapor permeation measurements were performed in a stainless steel tube module cell. The tubular membrane was placed inside the module cell and sealed by graphite cylindrical rings at both ends. A thermocouple was inserted into the module cell and placed close to the inner surface of the membrane. The effective membrane area was 6.28 cm^2. Vapor permeation tests were performed at 373, 398, and 423 K. The composition of the feed water/IPA mixture was 45/55 kPa. The permeate side was swept with He of 300 cm^3 (STP) min^{-1}. The pressures on both the retentate and permeate sides of membrane were atmospheric. Both the permeate and retentate were analyzed for its composition by means of gas chromatography (GC, Shimadzu GC-8A).

Permeance was calculated using eq 1

$$\text{permeance}[\text{mol m}^{-2}\text{s}^{-1}\text{ Pa}^{-1}] = uA^{-1}\Delta p^{-1} \quad (1)$$

where u is the amount of flow rate [mol s^{-1}], A is the effective membrane area [m^2], and Δp is the partial pressure difference between the feed and the permeate sides [Pa].

Separation factor was calculated using eq 2

$$\alpha_{W/I} = (Y_W/Y_I)/(X_W/X_I) \quad (2)$$

where X_W and X_I are the mole fractions of water and IPA in the feed, respectively, and Y_W and Y_I are the mole fractions of water and IPA in the permeate, respectively.

■ ASSOCIATED CONTENT

Supporting Information

The Supporting Information is available free of charge at https://pubs.acs.org/doi/10.1021/acsomega.1c00513.

Degassing procedure; XRD pattern of membrane on planar and porous support; and weight gains of planar support during seeding in different slurry concentrations (PDF)

■ AUTHOR INFORMATION

Corresponding Author

Masahiko Matsukata − *Department of Applied Chemistry, Waseda University, Tokyo 169-8555, Japan; Advanced Research Institute for Science and Engineering, Waseda University, Tokyo 169-8555, Japan;* orcid.org/0000-0003-0737-2117; Email: mmatsu@waseda.jp

Authors

Yasushi Sekine − *Department of Applied Chemistry, Waseda University, Tokyo 169-8555, Japan; Advanced Research Institute for Science and Engineering, Waseda University, Tokyo 169-8555, Japan;* orcid.org/0000-0001-6645-1961

Eiichi Kikuchi − *Department of Applied Chemistry, Waseda University, Tokyo 169-8555, Japan*

Motomu Sakai − *Department of Applied Chemistry, Waseda University, Tokyo 169-8555, Japan; Advanced Research Institute for Science and Engineering, Waseda University, Tokyo 169-8555, Japan;* orcid.org/0000-0003-4019-3479

Bharathi Subramanian − *Department of Applied Chemistry, Waseda University, Tokyo 169-8555, Japan; Advanced Research Institute for Science and Engineering, Waseda University, Tokyo 169-8555, Japan;* orcid.org/0000-0002-6870-2645

Makoto Toyoda − *Department of Applied Chemistry, Waseda University, Tokyo 169-8555, Japan*

Taisuke Furuhata − *Department of Applied Chemistry, Waseda University, Tokyo 169-8555, Japan*

Complete contact information is available at: https://pubs.acs.org/10.1021/acsomega.1c00513

Author Contributions

The manuscript was written through contributions of all authors. All authors have given approval to the final version of the manuscript.

Notes

The authors declare no competing financial interest.

■ ACKNOWLEDGMENTS

This work was financially supported by NEDO, Japan, as a research program entitled "Development of Fundamental Technologies for Green and Sustainable Chemical Processes: Fundamental development of ordered-nanoporous membranes for highly-refined separation technology".

■ REFERENCES

(1) Pina, M. P.; Mallada, R.; Arruebo, M.; Urbiztondo, M.; Navascues, N.; de la Iglesia, O.; Santamaria, J. Zeolite Films and Membranes. Emerging applications. *Microporous and Mesoporus Mater.* **2011**, *144*, 19−27.

(2) Cho, J.; Jeon, J. Optimization study on the azeotropic distillation process for isopropyl alcohol dehydration. *Korean J. Chem. Eng.* **2006**, *23*, 1−7.

(3) Lipnizki, F.; Field, R. W.; Ten, P. Pervaporation − based hybrid process: a review of process design, applications, and economics. *J. Membr. Sci.* **1999**, *153*, 183−210.

(4) Wang, Y.; Jiang, L. Y.; Matsuura, T.; Chung, T. S.; Goh, S. H. Investigation of the fundamental differences between polyamide−imide (PAI) and polyetherimide (PEI) membranes for isopropanol dehydration via pervaporation. *J. Membr. Sci.* **2008**, *318*, 217−226.

(5) Wang, Y.; Goh, S. H.; Chung, T. S.; Na, P. Polyamide−imide / polyetherimide dual−layer hollow fiber membranes for pervaporation dehydration of C_1 − C_4 Alcohols. *J. Membr. Sci.* **2009**, *326*, 222−233.

(6) Teoh, M. M.; Chung, T. S.; Wang, K. Y.; Guiver, M. D. Exploring torlon/P84 copolyamide−imide blended hollow fibers and their chemical cross−linking modifications for pervaporation dehydration of isopropanol. *Sep. Purif. Technol.* **2008**, *61*, 225−229.

(7) Higuchi, A.; Yoshikawa, M.; Guiver, M. D.; Robertson, G. P. Vapor permeation and pervaporation of aqueous 2−propanol solutions through the torlon poly (amide imide) membrane. *Sep. Sci. Technol.* **2005**, *40*, 2697−2707.

(8) Yoshikawa, M.; Higuchi, A.; Ishikawa, M.; Guiver, M. D.; Robertson, G. P. Vapor permeation and pervaporation of aqueous 2−propanol solutions through gelatin/torlon poly (amide imide) blended membrane. *J. Membr. Sci.* **2004**, *243*, 89−95.

(9) van Gemert, R. W.; Cuperus, F. P. Newly developed ceramic membranes for dehydration and separation of organic mixtures by pervaporation. *J. Membr. Sci.* **1995**, *105*, 287−291.

(10) van Veen, H. M.; Delft, Y. C.; Engelen, C. W. R.; Pex, P. P. A. C. Dewatering of organics by pervaporation with silica membranes. *Sep. Purif. Technol.* **2001**, *22*−*23*, 361−366.

(11) Cuperus, F. P.; Germert van, R. W. Dehydration using ceramic silica pervaporation membranes- the influence of hydrodynamic conditions. *Sep. Purif. Techol.* **2002**, *27*, 225−229.

(12) Qiao, X.; Chung, T.; Rajagopalan, R. Zeolite filled P84 co−polyimide membranes for dehydration of isopropanol through pervaporation process. *Chem. Eng. Sci.* **2006**, *61*, 6816−6825.
(13) Van Gestel, T.; Sebold, D.; Kruidhof, H.; Bouwmeester, H. J. M. ZrO_2 and TiO_2 membranes for nanofiltration and pervaporation part 2. Development of ZrO_2 and TiO_2 top layers for pervaporation. *J. Membr. Sci.* **2008**, *318*, 413−421.
(14) Yang, J.; Yoshioka, T.; Tsuru, T.; Asaeda, M. Pervaporation characteristics of aqueous−organic solutions with microporous SiO_2−ZrO_2 membranes: experimental study on separation mechanism. *J. Membr. Sci.* **2006**, *284*, 205−213.
(15) Asaeda, M.; Sakou, Y.; Yang, J.; Shimasaki, K. Stability and performance of porous silica−zirconia composite membranes for pervaporation of aqueous organic solutions. *J. Membr. Sci.* **2002**, *209*, 163−175.
(16) Sekulić, J.; Luiten, M. W. J.; ten Elshof, J. E.; Benes, N. E.; Keizer, K. Microporous silica and doped silica membrane for alcohol dehydration by pervaporation. *Desalination* **2002**, *148*, 19−23.
(17) Kondo, M.; Yamamura, T.; Yukitake; Matsuo, Y.; Kita, H.; Okamoto, K. IPA purification for lens cleaning by vapor permeation using zeolite membrane. *Sep. Purif. Technol.* **2003**, *32*, 191−198.
(18) Sommer, S.; Melin, T. Influence of operation parameters on the separation of mixtures by pervaporation and vapor permeation with inorganic membranes. part 2: purely organic systems. *Chem. Eng. Sci.* **2005**, *60*, 4525−4533.
(19) Kusakabe, K.; Kuroda, T.; Murata, A.; Morooka, S. Formation of a Y−type zeolite membrane on a porous α-alumina tube for gas separation. *Ind. Eng. Chem. Res.* **1997**, *36*, 649−655.
(20) Gu, X.; Dong, J.; Nenoff, T. M. Synthesis of structure directing agent−free FAU−type zeolite membranes and separation for dry and moist CO_2/N_2 mixtures. *Ind. Eng. Chem. Res.* **2005**, *44*, 937−944.
(21) Hasegawa, Y.; Watanabe, K.; Kusakabe, K.; Morooka, S. The separation of CO_2 using Y−type zeolite membranes ion−exchanged with alkali metal cations. *Sep. Purif. Technol.* **2001**, *22*−*23*, 319−325.
(22) Kita, H.; Fuchida, K.; Horita, T.; Asamura, H.; Okamoto, K. Preparation of faujasite membranes and their permeation properties. *Sep. Purif. Tech.* **2001**, *25*, 261−268.
(23) Kumakiri, I.; Yamaguchi, T.; Nakao, S. Preparation of zeolite A and faujasite membranes from a clear solution. *Ind. Eng. Chem. Res.* **1999**, *38*, 4682−4688.
(24) Kuzniatsova, T.; Kim, Y.; Shqau, K.; Dutta, P. K.; Verweij, H. Zeta potential measurements of zeolite Y: Application in homogeneous deposition of particle coatings. *Microporous Mesoporous Mater.* **2007**, *103*, 102−107.
(25) Chen, C.; Cheng, Y.; Peng, Li.; Zhang, C.; Wu, Z.; Gu, X.; Wang, X.; Murad, S. Fabrication and stability exploration of hollow fiber mordenite zeolite membrane for isopropanol/water mixture separation. *Microporous Mesoporous Mater.* **2019**, *274*, 347−355.
(26) Liu, B.; Kita, H.; Yogo, H. Preparation of Si-rich LTA zeolite membrane using organic template free solution for methanol dehydration. *Sep. Purif. Technol.* **2020**, *239*, No. 116533.
(27) Xu, X.; Zhou, C.; Wang, S.; Huang, A. Copper-exchanged LTA zeolite membrane with enhanced ethanol water flux for ethanol dehydration. *Chinese Chem. Lett.* **2019**, *30*, 1204−1206.

https://doi.org/10.1021/acsomega.1c00513
ACS Omega 2021, 6, 9834−9842